*nanomaterials*

MDPI

*Article*

# Synthesis of p-$Co_3O_4$/n-$TiO_2$ Nanoparticles for Overall Water Splitting under Visible Light Irradiation

**Qiang Zhang [1,2,†], Zhenyin Hai [1,†], Aoqun Jian [2], Hongyan Xu [3], Chenyang Xue [1,*] and Shengbo Sang [2,*]**

1 Key Laboratory of Instrumentation Science and Dynamic Measurement of Ministry of Education, North University of China, Taiyuan 030051, China; zhangq0902@163.com (Q.Z.); zhenyinhai0351@gmail.com (Z.H.)

2 MicroNano System Research Center, Key Laboratory of Advanced Transducers and Intelligent Control System of Ministry of Education and Shanxi Province & College of Information Engineering, Taiyuan University of Technology, Taiyuan 030024, China; jianaoqun@tyut.edu.cn

3 School of Materials Science and Engineering, North University of China, Taiyuan 030051, China; xuhongyan@foxmail.com

* Correspondence: xuechenyang@nuc.edu.cn (C.X.); sangshengbo@tyut.edu.cn (S.S.); Tel.: +86-351-392-1756 (C.X.); +86-375-349-2863 (S.S.)

† These authors contributed equally to this work.

Academic Editors: Hongqi Sun and Zhaohui Wang
Received: 27 May 2016; Accepted: 15 July 2016; Published: 27 July 2016

**Abstract:** p-$Co_3O_4$/n-$TiO_2$ nanoparticles (~400 nm) for photocatalysis were prepared via carbon assisted method and sol-gel method in this work. The paper also studied the application of visible light illuminated p-$Co_3O_4$/n-$TiO_2$ nanocomposites cocatalyst to the overall pure water splitting into $H_2$ and $O_2$. In addition, the $H_2$ evolution rate of the p-$Co_3O_4$/n-$TiO_2$ nanocomposites is 25% higher than that of the pure $Co_3O_4$ nanoparticles. Besides, according to the results of the characterizations, the scheme of visible light photocatalytic water splitting is proposed, the $Co_3O_4$ of the nanocomposites is excited by visible light, and the photo-generated electrons and holes existing on the conduction band of $Co_3O_4$ and valence band of $TiO_2$ have endowed the photocatalytic evolution of $H_2$ and $O_2$ with higher efficiency. The optimal evolution rate of $H_2$ and $O_2$ is 8.16 μmol/h· g and 4.0 μmol/h· g, respectively.

**Keywords:** nanocomposites; photocatalysis; visible light; overall water splitting

## 1. Introduction

The sharp increase in global energy consumption makes efficient utilization of solar energy more urgent [1]. Therefore, overall water splitting under visible light has received much attention for production of renewable hydrogen from water [2]. To improve the efficiency of the hydrogen production, researchers work hard on modifying the nanomaterials [3–6]. Moreover, doping rare metals on semiconductor nanomaterials, changing the morphology of the nanomaterials and synthesis of complex nanomaterials are hot means that can be employed to improve the photocatalytic activity [7–18]. Maeda studied the photocatalytic activity of Rutile $TiO_2$ doped by Ru, Rh, Ir, Pt or Au, with the results showing that the most water splitting amount of $H_2$ and $O_2$ for 4 h is 56.6 μmol and 26.5 μmol, respectively, when Pt doping amount is at 1 wt. % [7]. The water splitting amount of $H_2$ for 8 h is 2750 μmol, which is photocatalyzed by 3D ZnO microspheres prepared by Guo [8]. $Co_3O_4$ Quantum Dots show excellent performance on photocatalytic water splitting that the water splitting amount of $H_2$ and $O_2$ is 0.79 μmol/h and 0.4 μmol/h, respectively [18]. Meanwhile, some

nanomaterials ($La_2Ti_2O_7$, $PbTiO_3$, $SrTiO_3$, etc.) also play important roles in water splitting [9–17]. The water splitting amount of $H_2$ is 166.67 μmol/h· g when Au and reducing graphene oxide doped $La_2Ti_2O_7$ act as photocatalyst [11]. However, the methods of synthesizing the photocatalyst mentioned above are complex, along with high cost of doping Pt. Therefore, this paper aims to design a photocatalyst with relatively high activity via easy methods and low cost.

Many researches focus on enhancing the visible light absorption of $TiO_2$, but the main problems of these methods are high cost, complex processes and compositions [19–22]. Band gap of the $Co_3O_4$ nanomaterials is very close to the wavelength of visible light, so $Co_3O_4$ nanomaterials can be excited by visible light. However, typically, the p type $Co_3O_4$ semiconductor cannot be used on overall water splitting [23]. Some studies researched on changing the band gap of $Co_3O_4$; nevertheless, the constraints of these methods are high cost and difficult controlling processes [12–17,24]. Therefore, a new p-$Co_3O_4$/n-$TiO_2$ photococatalyst is designed for overall pure water splitting under visible light irradiation, and the $Co_3O_4$ and $TiO_2$ nanoparticles is, to the best of our knowledge, combined in nano-scale for the first time [25–27]. According to the band edge positions of $TiO_2$-$Co_3O_4$ nanocomposites, the excited electrons on the conduction band of the p-type $Co_3O_4$ transfer to that of the n-type $TiO_2$, and simultaneously holes on the valence band of n-$TiO_2$ can be transferred to that of p-$Co_3O_4$ under the potential of the band energy difference. The migration of photogenerated carriers can be promoted by the internal field, which results in existence fewer barriers. Therefore, the electron–hole pairs recombination of can be reduced, and the photocatalytic reaction can be improved greatly [28,29].

Many efforts have been devoted to synthesizing $Co_3O_4$ with well-controlled dimensionality, sizes, and crystal structure [30–33]. Wang et al. reported a carbon-assisted carbothermal method to synthesize the single-crystalline $Co_3O_4$ octahedral cages with tunable surface aperture [30]. Moreover, with the carbon spheres obtained through hydrothermal carbonization as the sacrificial template, Du et al. have successfully synthesized $Co_3O_4$ hollow spheres by a one-pot calcinations method [31]. Furthermore, Zhang et al. described the synthesis of high purity octahedral $Co_3O_4$ with the help of carbon materials using one-step microwave reaction [33]. Based on the researches mentioned above, p-$Co_3O_4$ nanoparticles are prepared through a more facile and environment-friendly carbon-assisted method using degrease cotton, which have been reported by our group in 2015 [23]. $TiO_2$ nanoparticles were composed via gol-sel method [34]. Besides, the paper presented the study on the application of visible light illuminated p-$Co_3O_4$/n-$TiO_2$ nanocomposites cocatalyst to the overall pure water splitting into $H_2$ and $O_2$, and the $H_2$ evolution rate of the p-$Co_3O_4$/n-$TiO_2$ nanocomposites is 25% higher than that of the pure $Co_3O_4$ nanoparticles. In addition, the scheme of visible light photocatalytic water splitting is proposed based on the results of the characterizations.

## 2. Experimental Section

### *2.1. Synthesis*

All chemicals were reagent grade and used without further purification. Cobalt nitrate, tetra-butyl ortho-titanate (TBOT), ethanol, hydrochloric acid and nitric acid were purchased from Sinopharm Chemical Reagent Co. Ltd. (Shanghai, China). Commercial degreasing cotton (Pagoda Medical Devices Co., Ltd., Dingzhou, China) was used as the reactant. Deionized water of 18.25 MΩ was purified through an ultra-pure (UPR) system (Xi'an You Pu Equipment Co., Ltd., Xi'an, China).

The $Co_3O_4$ nanoparticles (0.06 mol) were prepared via environmentally friendly carbon-assisted method, as reported in the previous article [23]. Specifically, immersed into 20 mL $Co(NO_3)_2$ pink solution (3 mol/L), 1.5 g degreasing cotton was then kept in an ultrasonic bath for 10 min in order to get a good dispersion of $Co^{2+}$ on the surface of degreasing cotton. Then, the treated degreasing cotton was collected and transferred into a quartz petri dish in the tube furnace (OTF-1200X-III, Hefei Ke Jing Materials Technology Co., Ltd., Hefei, China) and kept at 600 °C for 2 h in the air. Besides, the $Co_3O_4$ powders were cooled to the room temperature naturally.

The $Co_3O_4$ nanoparticles were composed with 0.06 mol $TiO_2$ through the following steps: The $Co_3O_4$ powders were put into a beaker with solation whose volume ratio of TBOT, nitric acid, alcohol and deionized water were 30.3:0.6:12.5:1 with continuous stirring. Moreover, a multifunctional magnetic stirrer (MPL-CJ-88) was used to stir and heat the solution (Jintandadi Automation Factory, Jintan, China). With the help of ultrasonic bath (KQ-2500DE) from Kunshan Shumei Ultrasonic Instrument Co. Ltd. (Kunshan, China), the beaker of solution and 10 g of particles (the obtained $TiO_2$ solution is about 150 mL) were ultra-sonicated, after which it was stirred for 30 min. The wet particles were heated at 500 °C for 2 h after being reacted for three hours. After milling with an agate mortar, the $TiO_2$-$Co_3O_4$ composite was finally obtained.

### 2.2. Characterization

The crystal structure of the sample was measured through X-ray diffraction (XRD, a Bruker D8, λ = 1.5406 Å) (Bruker (Beijing) Technology Co., Ltd., Beijing, China) in the 2θ of 10°–80° with a scan rate of 10°/min and Cu Kα radiation, at 40 KV. Chemical composition analysis was carried out using X-ray photoelectron spectroscopy (XPS). This XPS was collected using an ESCALAB 250Xi spectrometer (Shanghai Hu Yueming scientific instruments Ltd., Shanghai, China) with a standard Al Kα radiation which was provided with the binding energies calibrated based on the contaminant carbon (C1s = 284.6 eV). The morphology was observed by transmission electron microscopy (TEM, JEOL JEM-2011) (Guangzhou Office of Japan Electronics Co., Ltd., Guangzhou, China). Furthermore, with the presence of BET (Brunauer-Emmet-Teller) and BJH (Barrett-Joyner-Halenda), specific surface areas and pore size distributions were computed from the results of $N_2$ physisorption at 77 K (Micromeritics ASAP 2020) (Micromerics (Shanghai) Instrument Co., Ltd., Shanghai, China). A Cary 300 Scan Ultraviolet–visible (UV-Vis) spectrophotometer (Shanghai Precision Instrument Science Co., Ltd., Shanghai, China) was employed to record the UV-Vis diffuse reflectance spectra (DRS) in a region of 200 to 800 nm.

### 2.3. Photocatalysis

The photocatalytic activity for the overall pure water splitting into $H_2$ and $O_2$ was estimated under visible light condition. The diagram of visible light water splitting system is shown in Figure 1.


**Figure 1.** Diagram of visible light water splitting system.

Typically, 0.02 g photocatalyst was added into the solution (~200 mL) containing 200 mL pure water solution. After put in an ultrasonic stirring for 20 min, purged by Ar gas for 20 min, the mixture was then irradiated under visible light with magnetic stirring. A 300 W Xe arc lamp (LSH-A500, KaifengHxsei Science Instrument Co. Ltd., Kaifeng, China) with UV cut-off filters (420 nm) was used as the light source. In addition, the hydrogen produced was analyzed by a gas chromatography (GC-9890B, Shanghai Linghua Instrument Co. Ltd., Shanghai, China) equipped with a thermal

conductivity detector and a stainless steel column packed with molecular sieve (5 A). Ar gas (99.999%) was used as the carrier gas.

## 3. Results and Discussion

The XRD patterns of the $Co_3O_4$ are shown in Figure 2a. All peaks have a good agreement with the standard spinel cubic $Co_3O_4$ spectrum (JCPDS No. 42-1467), while there are no impurity peaks found in the XRD patterns. The result suggests that the well-crystallized $Co_3O_4$ with high purity sample is produced. According to Scherrer's formula, $D = 0.89\lambda/(B\cos\theta)$ (where $D$ is the average dimension of crystallites; $\lambda$ is the X-ray wavelength; $\theta$ is the Bragg Angle; and $B$ is the pure diffraction broadening of a peak at half-height, which is calculated according to the data of XRD spectrum), the crystalline size of $Co_3O_4$, calculated from the strongest peak, locating at (311) plane, are estimated to be 51.64 nm.

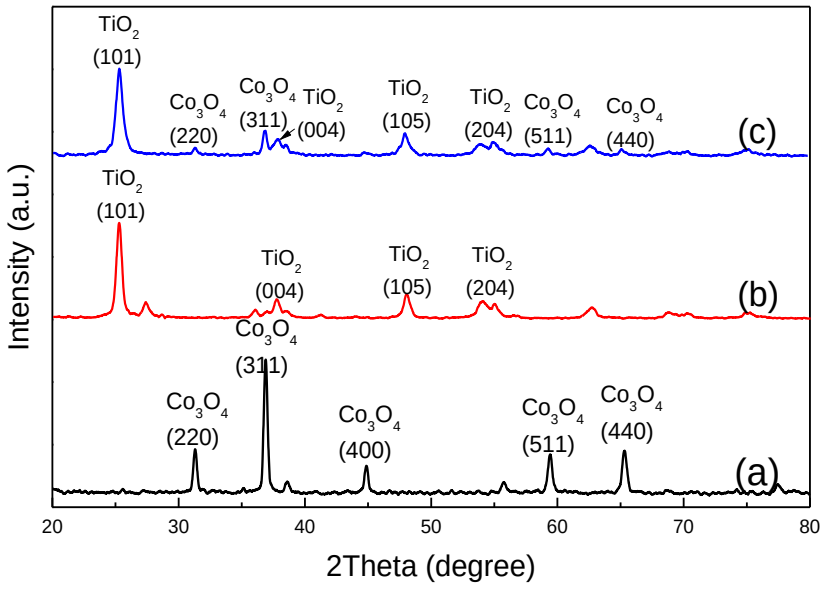


**Figure 2.** X-ray diffraction (XRD) pattern of the: (**a**) $Co_3O_4$ sample; (**b**) $TiO_2$ sample; and (**c**) $TiO_2$-$Co_3O_4$ sample. a.u.: any unit.

Figure 2b demonstrates that anatase (JCPDS No. 21-1272) with high purity sample is obtained via gol-sel method. According to Scherrer's formula mentioned above, the crystalline size of $TiO_2$ is estimated to be 22.48 nm. The wider peaks in Figure 2c have shown bigger composites sizes. To confirm all of the nanoparticles contain both $Co_3O_4$ and $TiO_2$, the $TiO_2$ are compounded after the obtaining of bigger size $Co_3O_4$. In addition, avoiding the visible light absorber $Co_3O_4$ being coated completely, the mol ratio of these two materials is controlled strictly as 1:1. As demonstrated in Figure 2c, there are no facets existing other than $Co_3O_4$ and $TiO_2$. However, the $Co_3O_4$ peaks are much weaker than that of $TiO_2$, with the possible reason being that the $Co_3O_4$ is partially coated by $TiO_2$.

To identify the chemical state of the nanocomposite, the X-ray photoelectron spectroscopy (XPS) was measured (Figure 3). By using adventitious carbon at 284.8 eV, the XPS spectra were corrected for sample charging. The Co2p orbital showed splitting peaks at 794.7 and 779.6 eV, representing Co2p 3/2 and Co2p 1/2 [35]. The Ti2p orbital showed peaks at 464.0 and 458.2 eV, thus indicating the Ti2p 3/2 and Ti2p 1/2 [36,37]. As for the XPS of O1s at 531.6 and 529.5 eV, it would indicate the presence of adsorbed water and oxygen in the near-surface region [13]. The strong peak of C1S centers at 284.5 eV can be assigned to elemental carbon, which has given rise to the incomplete burning of degreasing cotton; in contrast, the other two peaks appeared at 285.8 and 288.6 eV, respectively, which are ascribed to the O=C–O bonds and $(CHO)_x$ from insufficient combustion residual degreasing cotton [38]. No Co–C or Ti–C band is found in the spectra, which means that the conjunctions of

the nanocomposites are not affected by C. Therefore, according to the results of the XPS spectra, the $TiO_2$-$Co_3O_4$ sample is composed only by $TiO_2$, $Co_3O_4$ and residual degreasing cotton, which is consisted with the XRD results.

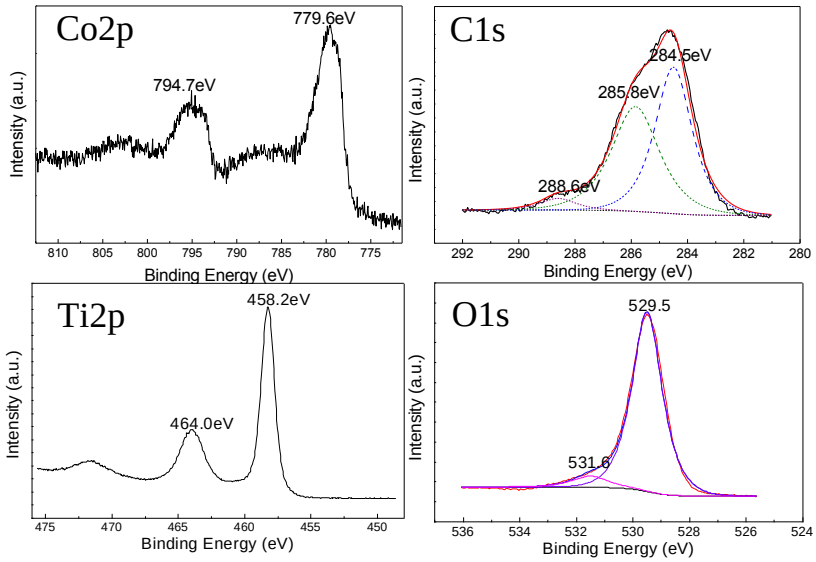


**Figure 3.** X-ray photoelectron spectroscopy (XPS) spectra of the $TiO_2$-$Co_3O_4$ sample.

The morphology and structure of the samples are observed via TEM, with the results presented in Figure 4. Figure 4a shows that the $Co_3O_4$ nanospheres with a relatively uniform size of 60 nm are obtained. It can be seen that 20 nm $TiO_2$ nanoparticles compose the big group in Figure 4b, which is consistent with the calculation from XRD mentioned above. The Figure 4c is the TEM image of the $TiO_2$-$Co_3O_4$ sample. The darker part in Figure 3c is $Co_3O_4$ while the lighter part is $TiO_2$, which can be proved by both the synthetic procedures and the results of High Resolution Transmission Electron Microscopy (HRTEM) in Figure 4d–f. The $TiO_2$ accumulates around the $Co_3O_4$ incompletely, while the $TiO_2$ and the $Co_3O_4$ connected closely at the interface of the composite. The result of Figures 2–4 improves the elements and framework of the p-$Co_3O_4$/n-$TiO_2$ nanocomposites.

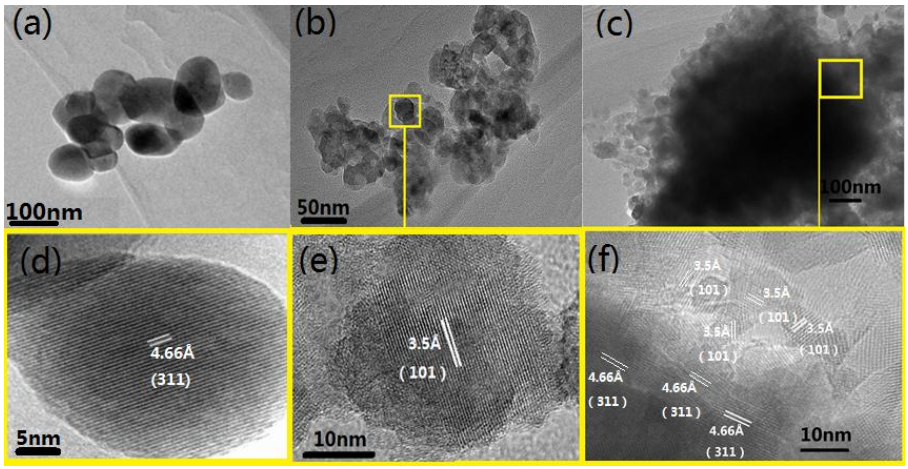


**Figure 4.** Transmission electron microscopy (TEM) images of: (**a**) the $Co_3O_4$ sample; (**b**) $TiO_2$ sample; and (**c**) $TiO_2$-$Co_3O_4$ sample. High Resolution Transmission Electron Microscopy (HRTEM) images of: (**d**) the $Co_3O_4$ sample; (**e**) $TiO_2$ sample; and (**f**) $TiO_2$-$Co_3O_4$ sample.

The $Co_3O_4$ is prepared firstly due to its clear edge and bigger size, while the mesoporous structure of the $TiO_2$ (which is shown as Figure 5) is another reason for the preparation of its designing on step two. Larger area of the conjunction and larger surface area of the composite for higher photocatalytic efficiency can be obtained in this way. Brunauer-Emmett-Teller (BET) surface areas and Barrett-Joyner-Halenda (BJH) pore size distributions of the $TiO_2$-$Co_3O_4$ are shown in Figure 5. According to the International Union of Pure and Applied Chemistry (IUPAC) classification, the isotherms exhibit type IV. As for the increase in the uptake of $N_2$ at intermediate pressure, which suggests the existence of mesoporous resulted from the interparticle space in the samples, it can facilitate the water accessibility to nanoparticles. According to the corresponding BJH pore size distribution curve, the pore size distribution has a relatively intense peak at ~10 nm. The BET surface area is calculated to be 39.64 $m^2/g$ and the average pore size is 3.83 nm. These results and the results of the TEM demonstrate the mesoporous existence on the $TiO_2$ layer of the composites. Furthermore, the relative higher surface area and the mesoporous structure will play a very important role in improving the water splitting efficiency of the composite.

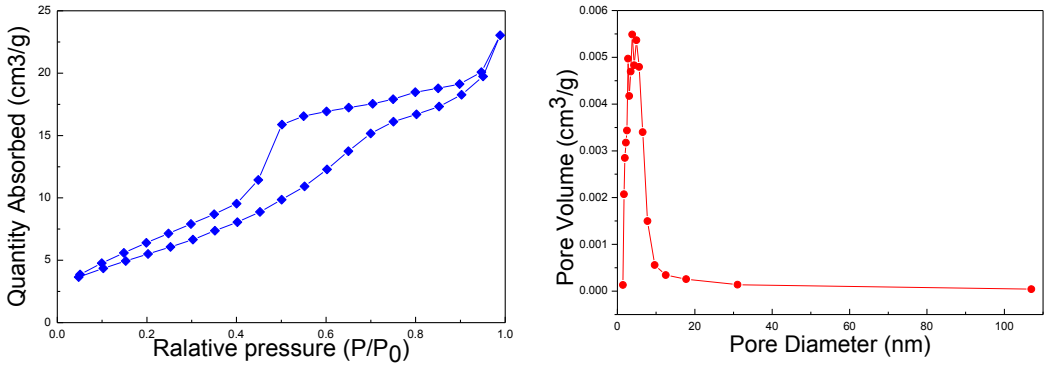


**Figure 5.** (**a**) Nitrogen adsorption–desorption isotherms; and (**b**) Barrett-Joyner-Halenda (BJH) pore size distributions of $TiO_2$-$Co_3O_4$ sample.

Investigation was conducted on the optical absorption properties of the $TiO_2$ nanoparticles, $Co_3O_4$ nanoparticles and $TiO_2$-$Co_3O_4$ heterostructures at room temperature by UV-Vis spectroscopy, as shown in Figure 6a. Broad background absorption in the visible light region can be observed for $Co_3O_4$ (Figure 6a, curve 1), while there is no absorption invisible light region for $TiO_2$ (Figure 6a curve 2). However, the absorption of the $TiO_2$-$Co_3O_4$ composite in the visible light region can achieve great improvement owing to the $Co_3O_4$ (Figure 6a curve 3). This result illustrates that the $TiO_2$-$Co_3O_4$ composite can be irradiated by visible light. Importantly, Figure 6b shows the valence-band XPS spectra of $TiO_2$ and $Co_3O_4$, clearly indicating that the valence band maximum of $TiO_2$ and $Co_3O_4$ are 2.4 and 0.6 eV. In addition, according to that the UV-Vis spectroscopy of $Co_3O_4$, the bandgap value calculated is 1.9 eV (Figure 6c) while the bandgap Eg value of $TiO_2$ is 3.2 eV (Figure 6d). Based on the above results, the schematic diagram of the water splitting reaction of the $TiO_2$-$Co_3O_4$ heterostructures is shown as Figure 6e. When $Co_3O_4$ semiconductor absorbs visible light photons, electrons in the valence band are excited to the conduction band. As a result, excited electrons and holes are generated in the conduction and valence bands of the composite, respectively. These photogenerated carriers drive reduction and oxidation reactions. The reduction of water to hydrogen and oxidation of reduced redox mediators occurs on $Co_3O_4$ and $TiO_2$ concurrently with the reduction of oxidized redox mediators and oxidation of water to oxygen on the $TiO_2$ [2]. According to the band edge position, the excited electrons on the conduction band of the p-type $Co_3O_4$ transfer to that of the n-type $TiO_2$, and simultaneous holes on the valence band of n-$TiO_2$ can be transferred to that of p-$Co_3O_4$ under the potential of the band energy difference. The migration of photogenerated carriers can be promoted by the internal

field, so barely any barrier exists. Therefore, the electron–hole pairs recombination can be reduced, and the p-n junction has a significant impact on the efficiency of photocatalytic water splitting.

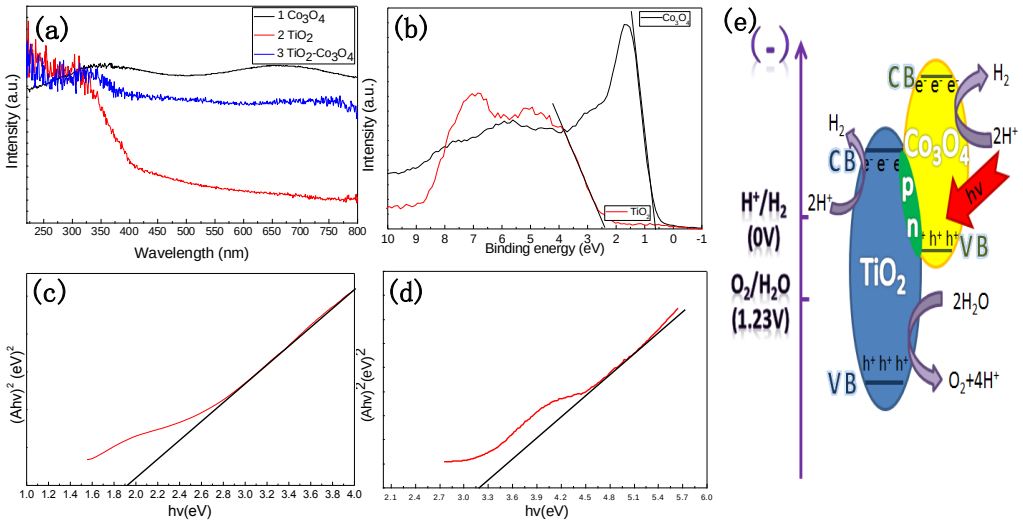


**Figure 6.** (**a**) Ultraviolet–visible (UV-Vis) spectra; and (**b**) Valence-band XPS spectra of $TiO_2$ and $Co_3O_4$ nanoparticles. $(Ahv)^2$–hv curve of: (**c**) $Co_3O_4$ nanoparticles; and (**d**) $TiO_2$ nanoparticles. (**e**) Schematic diagram of the water splitting reaction of the $TiO_2$-$Co_3O_4$ heterostructures.

The results of the measurements of $H_2$ evolution through direct photocatalytic water splitting with $Co_3O_4$ nanocomposites under visible light are shown as Figure 7. The $H_2$ evolution rates are 6.5 μmol/h· g, as shown in Figure 7.

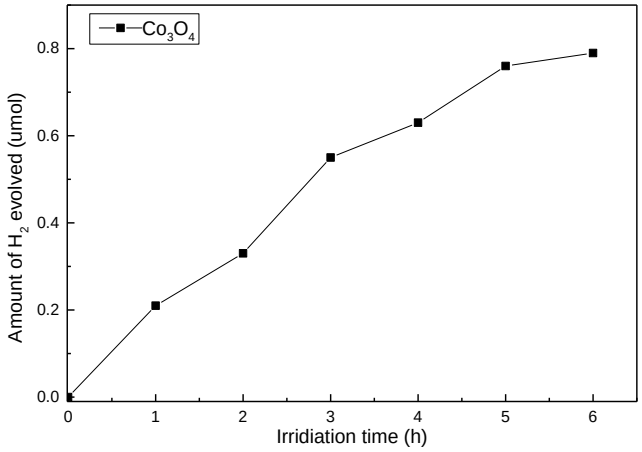


**Figure 7.** Photocatalytic $H_2$ evolution on $Co_3O_4$ nanocomposites under visible-light irradiation using 0.02 g photocatalyst suspended in 200 mL pure water solution in a Pyrex glass cell.

The measurements results of the $H_2$ and $O_2$ evolution through direct photocatalytic water splitting with $Co_3O_4$-$TiO_2$ nanocomposites under visible light are shown in Figure 8. The $H_2$ and $O_2$ evolution rates are 8.16 μmol/h· g and 4.0 μmol/h· g, respectively, as shown in Figure 8a. The approximated 2:1 of the $H_2$ and $O_2$ generation ratio demonstrate the $Co_3O_4$-$TiO_2$ nanocomposites capability for the overall water splitting. Due to the photoreduction of $O_2$ via a reverse reaction during water splitting, the slight deviation of the $H_2$:$O_2$ ratio from the ideal stoichiometric value could thus be acquired. The hydrogen peroxide was formed as an oxidation product, and molecular oxygen (another oxidation product) adsorbed too intimately on the surface of photocatalyst so as to desorb the gas phase, thus

resulting in the lack of $O_2$ [7,19]. Through the comparison between Figures 7 and 8a, it can be seen that the $H_2$ evolution rate of the p-$Co_3O_4$/n-$TiO_2$ nanocomposites is 25% higher than that of the pure $Co_3O_4$ nanoparticles. This result illustrates the mechanism in the way that the electron–hole pairs recombination can be reduced due to the structure of the p-$Co_3O_4$/n-$TiO_2$ nanocomposites, while the p-n junction has a significant impact on the efficiency of photocatalytic water splitting. Figure 8b shows that the $H_2$ and $O_2$ evolution rates are 7.67 μmol/h· g and 3.92 μmol/h· g after being recycled five times. The slight reduction of the gas generation is resulted by the quality loss caused by powders cleaning and drying; additionally, the mesoporous structure of the nanomaterials makes the water molecules difficult to be removed thoroughly. Together, the capability of the $Co_3O_4$-$TiO_2$ nanocomposites for the overall water splitting is demonstrated by the measurements of $H_2$ and $O_2$ evolution under visible light.

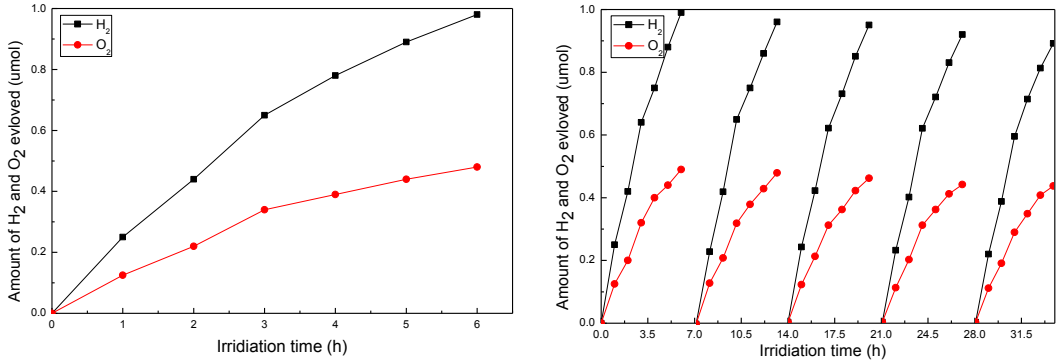


**Figure 8.** (**a**) Photocatalytic $H_2$ and $O_2$ evolution on $Co_3O_4$-$TiO_2$ nanocomposites under visible-light irradiation using 0.02 g photocatalyst suspended in 200 mL pure water solution in a Pyrex glass cell; and (**b**) cycling measurements of $H_2$ and $O_2$ evolution through direct photocatalytic water splitting with $Co_3O_4$-$TiO_2$ nanocomposites under visible light.

The gas generation rate comparison result is not precise because the light source and the sacrificial agent are different according to different researches. Therefore, a comparison was made of our results with some of the other works on pure water splitting under visible light. As concluded in Table 1, the gas generation rate of our nanocomposites is in the medium level. However, the preparation method of $Co_3O_4$ Quantum Dot [12] and Pt-$TiO_2$ [7] are hard to control, and, needless to say, high cost. Besides, the materials of p-$LaFeO_3$/$Fe_2O_3$ [39] are uncommon, and the treating temperature of Co-$TiO_2$ preparation is extremely high (~1100 °C) [19]. The simple preparation method of p-$Co_3O_4$/n-$TiO_2$ nanocomposites used in this work is environmentally friendly. In conclusion, the p-$Co_3O_4$/n-$TiO_2$ nanocomposites presented in this paper has a relatively high photocatalytic activity in terms of its facilitative methods.

**Table 1.** Research status of photocatalytic water splitting.

| Reference | Materials | Light Source | $H_2$ Amount | $O_2$ Amount | Sacrificial Agent |
|---|---|---|---|---|---|
| [8] | 3D ZnO microspheres | Visible light | 343.75 μmol/h | | Methanol, ethanol, formaldehyde |
| [12] | $Co_3O_4$ Quantum Dot | Visible light | 0.79 μmol/h | 0.4 μmol/h | none |
| [7] | Pt-$TiO_2$ | Ultraviolet light | 56.6 μmol/h | 26.5 μmol/h | none |
| [11] | Au@Pt-NLTO/rGO | Visible light | 166.67 μmol/h· g | | ethanol |
| [39] | p-$LaFeO_3$/$Fe_2O_3$ | Visible light | 80 μmol/h | 40 μmol/h | none |
| [19] | Co-$TiO_2$ | Visible light | 11 μmol/h· g | 5 μmol/h· g | none |
| [23] | $Co_3O_4$ | Visible light | 42.5 μmol/h· g | | ethanol |
| This work | $Co_3O_4$ | Visible light | 6.5 μmol/h· g | | none |
| This work | $Co_3O_4$-$TiO_2$ | Visible light | 8.16 μmol/h· g | 4.0 μmol/h· g | none |

## 4. Conclusions

In this work, carbon assisted method and sol-gel method were used to obtain the nanocomposite p-$Co_3O_4$/n-$TiO_2$ photocatalyst. Based on the XRD and XPS results, no other phase is generated other than $Co_3O_4$ and $TiO_2$. The formation of the p-$Co_3O_4$/n-$TiO_2$ conjunction is proven by the TEM and HRTEM investigations of $Co_3O_4$, $TiO_2$ and $Co_3O_4$-$TiO_2$ nanoparticles. The BET surface area and the average pore size of themes porous structure nanocomposite are 39.64 $m^2/g$ and 3.83 nm, respectively, which can be concluded through the Nitrogen adsorption-desorption curve. The schematic of visible light photocatalytic water splitting is surmised through the results of UV-Vis spectra, $(Ahv)^2$–hv curve and valence-band XPS spectra of $TiO_2$ and $Co_3O_4$ nanoparticles. The p-$Co_3O_4$/n-$TiO_2$ composites have a significant impact on the efficiency of photocatalytic water splitting. Finally, the results of visible light irradiating overall water splitting reaction can prove the photocatalytic activity of the p-$Co_3O_4$/n-$TiO_2$ nanocomposite. The optimal evolution rate of $H_2$ and $O_2$ is 8.16 μmol/g· L and 4.0 μmol/g· L, respectively. In addition, the $H_2$ evolution rate of the p-$Co_3O_4$/n-$TiO_2$ nanocomposites is 25% higher than that of the pure $Co_3O_4$ nanoparticles.

**Acknowledgments:** Project supported by the National Science Foundation for Young Scientists of China (Grant No. 61501408).

**Author Contributions:** Qiang Zhang, Zhenyin Hai, Aoqun Jian, Hongyan Xu, Chenyang Xue and Shengbo Sang designed the experiments; Qiang Zhang, Zhenyin Hai and Aoqun Jian performed the experiments; Hongyan Xu, Chenyang Xue and Shengbo Sang analyzed the data; Qiang Zhang and Shengbo Sang wrote the paper; all authors discussed the results and commented on the manuscript.

**Conflicts of Interest:** The authors declare no conflict of interest.

## References

1. Lewis, N.S.; Nocera, D.G. Powering the planet: Chemical challenges in solar energy utilization. *Proc. Natl. Acad. Sci. USA* **2006**, *103*, 15729–15735. [CrossRef] [PubMed]
2. Hisatomi, T.; Kubota, J.; Domen, K. Recent advances in semiconductors for photocatalytic and photoelectrochemical water splitting. *Chem. Soc. Rev.* **2014**, *43*, 7520–7535. [CrossRef] [PubMed]
3. Chen, H.; Cong, T.N.; Yang, W.; Tan, C.; Li, Y.; Ding, Y. Progress in electrical energy storage system: A critical review. *Prog. Nat. Sci.* **2009**, *19*, 291–312. [CrossRef]
4. Yang, P.; Tarascon, J.M. Towards systems materials engineering. *Nat. Mater.* **2012**, *11*, 560–563. [CrossRef] [PubMed]
5. Kanan, M.W.; Nocera, D.G. In situ formation of an oxygen-evolving catalyst in neutral water containing phosphate and $Co^{2+}$. *Science* **2008**, *321*, 1072–1075. [CrossRef] [PubMed]
6. Sun, K.; Jing, Y.; Li, C.; Zhang, X.F.; Aguinaldo, R.; Alireza, K.; Madsen, K.; Banu, K.; Zhou, Y.C.; Bando, Y.; et al. 3D branched nanowire heterojunction photoelectrodes for high-efficiency solar water splitting and $H_2$ generation. *Nanoscale* **2012**, *4*, 1515–1521. [CrossRef] [PubMed]
7. Maeda, K. Photocatalytic properties of rutile $TiO_2$ powder for overall water splitting. *Catal. Sci. Technol.* **2014**, *4*, 1949–1953. [CrossRef]
8. Guo, S.Y.; Zhao, T.J.; Jin, Z.Q.; Wan, X.M.; Wang, P.G.; Shang, J.; Han, S. Self-assembly synthesis of precious-metal-free 3D ZnO nano/micro spheres with excellent photocatalytic hydrogen production from solar water splitting. *J. Power Sources* **2015**, *293*, 17–22. [CrossRef]
9. Youngblood, W.J.; Lee, S.H.A.; Kobayashi, Y.; Hernandez-Pagan, E.A.; Hoertz, P.G.; Moore, T.A.; Moore, A.L.; Gust, D.; Mallouk, T.E. Photoassisted overall water splitting in a visible light-absorbing dye-sensitized photoelectrochemical cell. *J. Am. Chem. Soc.* **2009**, *131*, 926–927. [CrossRef] [PubMed]
10. Song, H.; Peng, T.; Cai, P.; Yi, H.; Yan, C. Hydrothermal synthesis of flaky crystallized $La_2Ti_2O_7$ for producing hydrogen from photocatalytic water splitting. *Catal. Lett.* **2007**, *113*, 54–58. [CrossRef]
11. Meng, F.; Cushing, S.K.; Li, J.; Hao, S.; Wu, N. Enhancement of Solar Hydrogen Generation by Synergistic Interaction of $La_2Ti_2O_7$ Photocatalyst with Plasmonic Gold Nanoparticles and Reduced Graphene Oxide Nanosheets. *ACS Catal.* **2015**, *5*, 1949–1955. [CrossRef]
12. Shi, N.; Cheng, W.; Zhou, H.; Fan, T.; Niederberger, M. Facile synthesis of monodisperse $Co_3O_4$ quantum dots with efficient oxygen evolution activity. *Chem. Commun.* **2015**, *51*, 1338–1340. [CrossRef] [PubMed]

13. Deng, S.; Chen, N.; Deng, D.; Li, Y.; Xing, X.; Wang, Y. Meso- and macroporous coral-like $Co_3O_4$ for VOCs gas sensor. *Ceram. Int.* **2015**, *41*, 11004–11012. [CrossRef]
14. Ge, B.; Li, K.; Fu, Z.; Pu, L.; Zhang, X. The addition of ortho-hexagon nano spinel $Co_3O_4$ to improve the performance of activated carbon air cathode microbial fuel cell. *Bioresour. Technol.* **2015**, *195*, 180–187. [CrossRef] [PubMed]
15. Li, L.; Tian, T.; Jiang, J.; Ai, L. Hierarchically porous $Co_3O_4$ architectures with honeycomb-like structures for efficient oxygen generation from electrochemical water splitting. *J. Power Sources* **2015**, *294*, 103–111. [CrossRef]
16. An, H.L.; An, G.H.; Ahn, H.J. Octahedral $Co_3O_4$/carbon nanofiber composite-supported Pt catalysts for improved methanol electrooxidation. *J. Alloys Compd.* **2015**, *645*, 317–321. [CrossRef]
17. Soomro, R.A.; Ibupoto, Z.H.; Sherazi, S.T.H.; Abro, M.I.; Willander, M.; Mahesar, S.A.; Kalwar, N.H. Glycine-assisted preparation of $Co_3O_4$ nanoflakes with enhanced performance for non-enzymatic glucose sensing. *Mater. Express* **2015**, *5*, 437–444. [CrossRef]
18. Zhang, N.; Shi, J.; Mao, S.S.; Guo, L. $Co_3O_4$ quantum dots: Reverse micelle synthesis and visible-light-driven photocatalytic overall water splitting. *Chem. Commun.* **2014**, *50*, 2002–2004. [CrossRef] [PubMed]
19. Zhang, D.; Yang, M. Band structure engineering of $TiO_2$ nanowires by n-p codoping for enhanced visible-light photoelectrochemical water-splitting. *Phys. Chem. Chem. Phys.* **2013**, *15*, 18523–18529. [CrossRef] [PubMed]
20. Shaban, Y.A.; Khan, S.U.M. Photoresponse of Visible Light Active CM-n-$TiO_2$, HM-n-$TiO_2$, CM-n-$Fe_2O_3$, and CM-p-$WO_3$ towards Water Splitting Reaction. *Int. J. Photoenergy* **2012**, *2012*. [CrossRef]
21. Odetola, C.; Trevani, T.L.; Easton, E.B. Enhanced activity and stability of Pt/$TiO_2$/carbon fuel cell electrocatalyst prepared using a glucose modifier. *J. Power Sources* **2015**, *294*, 254–263. [CrossRef]
22. Chen, X.; Liu, L.; Peter, Y.Y.; Mao, S.S. Increasing solar absorption for photocatalysis with black hydrogenated titanium dioxide nanocrystals. *Science* **2011**, *331*, 746–750. [CrossRef] [PubMed]
23. Gao, L.; Diwu, J.; Zhang, Q.; Xu, H.; Chou, X.; Tang, J.; Xue, C. A Green and Facile Synthesis of Carbon-incorporated $Co_3O_4$ Nanoparticles and Their Photocatalytic Activity for Hydrogen Evolution. *J. Nanomater.* **2015**, *2015*. [CrossRef]
24. Zhao, S.; Li, C.; Liu, J.; Liu, N.; Qiao, S.; Han, Y.; Liu, Y.; Huang, H.; Kang, Z. Carbon quantum dots/$SnO_2$-$Co_3O_4$ composite for highly efficient electrochemical water oxidation. *Carbon* **2015**, *92*, 64–73. [CrossRef]
25. Li, H.; Fei, G.T.; Fang, M.; Cui, P.; Guo, X.; Yan, P.; Zhang, L.D. Synthesis of urchin-like $Co_3O_4$ hierarchical micro/nanostructures and their photocatalytic activity. *Appl. Surf. Sci.* **2011**, *257*, 6527–6530. [CrossRef]
26. Kwak, G.; Hwang, J.; Cheon, J.Y.; Woo, M.H.; Jun, K.W.; Lee, J.; Ha, K.S. Preparation method of $Co_3O_4$ nanoparticles using ordered mesoporous carbons as a template and their application for fischer–tropsch synthesis. *J. Phys. Chem. C* **2013**, *117*, 1773–1779. [CrossRef]
27. Kuo, C.S.; Tseng, Y.H.; Huang, C.H.; Li, Y.Y. Carbon-containing nano-titania prepared by chemical vapor deposition and its visible-light-responsive photocatalytic activity. *J. Mol. Catal. A* **2007**, *270*, 93–100. [CrossRef]
28. Li, D.; Haneda, H.; Hishita, S.; Ohashi, N. Visible-light-driven NF-codoped $TiO_2$ photocatalysts. Optical characterization, photocatalysis, and potential application to air purification. *Chem. Mater.* **2005**, *17*, 2596–2602. [CrossRef]
29. Long, M.; Cai, W.; Cai, J.; Zhou, B.; Chai, X.; Wu, Y. Efficient photocatalytic degradation of phenol over $Co_3O_4$/$BiVO_4$ composite under visible light irradiation. *J. Phys. Chem. B* **2006**, *110*, 20211–20216. [CrossRef] [PubMed]
30. Wang, X.; Yu, L.; Wu, X.L.; Yuan, F.; Guo, Y.G.; Ma, Y.; Yao, J. Synthesis of single-crystalline $Co_3O_4$ octahedral cages with tunable surface aperture and their lithium storage properties. *J. Phys. Chem. C* **2009**, *113*, 15553–15558. [CrossRef]
31. Du, H.; Jiao, L.; Wang, Q.; Yang, J.; Guo, L.; Si, Y.; Wang, Y.J.; Yuan, H. Facile carbonaceous microsphere templated synthesis of $Co_3O_4$ hollow spheres and their electrochemical performance in supercapacitors. *Nano Res.* **2013**, *6*, 87–98. [CrossRef]
32. Liu, J.; Jiang, J.; Cheng, C.; Li, H.; Zhang, J.; Gong, H.; Fan, H.J. $Co_3O_4$ nanowire@$MnO_2$ ultrathin nanosheet core/shell arrays: A new class of high-performance pseudocapacitive materials. *Adv. Mater.* **2011**, *23*, 2076–2081. [CrossRef] [PubMed]

33. Zhang, P.; Hu, G.X.; Bao, S.J.; Guo, J.; Lei, C.; Cai, C.J.; Zeng, J.D.; Wang, R.Y. One step microwave synthesis and magnetic properties of $Co_3O_4$ octahedrons. *Mater. Lett.* **2012**, *83*, 195–197. [CrossRef]
34. Sugimoto, T.; Zhou, X.; Muramatsu, A. Synthesis of uniform anatase $TiO_2$ nanoparticles by gel–sol method: 3. Formation process and size control. *J. Colloid Interface Sci.* **2003**, *259*, 43–52. [CrossRef]
35. Li, J.; Lu, G.; Wu, G.; Mao, D.; Guo, Y.; Wang, Y.; Guo, Y. Effect of $TiO_2$ crystal structure on the catalytic performance of $Co_3O_4/TiO_2$ catalyst for low-temperature CO oxidation. *Catal. Sci. Technol.* **2014**, *4*, 1268–1275. [CrossRef]
36. Ernsberger, C.; Nickerson, J.; Smith, T.; Miller, A.E.; Banks, D. Low temperature oxidation behavior of reactively sputtered TiN by X-ray photoelectron spectroscopy and contact resistance measurements. *J. Vac. Sci. Technol. A* **1986**, *4*, 2784–2788. [CrossRef]
37. Rubinstein, R.Y.; Shapiro, A. *Discrete Event Systems: Sensitivity Analysis and Stochastic Optimization by the Score Function Method*; John Wiley & Sons Inc.: Hoboken, NJ, USA, 1993.
38. Zhang, S.; Li, X.; Chen, J.P. An XPS study for mechanisms of arsenate adsorption onto a magnetite-doped activated carbon fiber. *J. Colloid Interface Sci.* **2010**, *343*, 232–238. [CrossRef] [PubMed]
39. Yu, Q.; Meng, X.; Wang, T.; Liu, L.; Chang, K.; Liu, G.G.; Ye, J. A highly durable p-$LaFeO_3$/n-$Fe_2O_3$ photocell for effective water splitting under visible light. *Chem. Commun.* **2015**, *51*, 3630–3633. [CrossRef] [PubMed]